Copper(II) Complexes of Substituted Macrobicyclic Hexaamines: Combined Trigonal and Tetragonal Distortions

Paul V. Bernhardt,*[1] Richard Bramley,*[1] Lutz M. Engelhardt,*[2] Jack M. Harrowfield,*[2] David C. R. Hockless,*[1] Bohdan R. Korybut-Daszkiewicz,*[1] Elmars R. Krausz,*[1] Tammy Morgan,*[1] Alan M. Sargeson,*[1] Brian W. Skelton,*[2] and Allan H. White*[2]

Research School of Chemistry, Australian National University, Canberra, ACT 0200, Australia, and Department of Physical and Inorganic Chemistry, University of Western Australia, Nedlands, WA 6009, Australia

Received December 1, 1994[⊗]

The hexaamine complexes $[M\{(NH_3)_2sar\}]^{4+}$ and $[M\{(NMe_3)_2sar\}]^{4+}$ (M = Cu(II), Zn(II); sar = 3,6,10,13,16,-19-hexaazabicyclo[6.6.6]icosane) have been synthesized and characterized both spectroscopically and structurally. X-ray crystal structural analyses of $[Cu\{(NH_3)_2sar\}](NO_3)_4{\cdot}H_2O$ (monoclinic, $P2_1$, a 12.311(3) Å, b 12.338(4) Å, c 8.574(3) Å, β 93.91(3)°, $Z = 2$), $[Zn\{(NH_3)_2sar\}](NO_3)_4{\cdot}H_2O$ (monoclinic, $P2_1$, a 12.365(4) Å, b 12.396(7) Å, c 8.587(4) Å, β 94.13(3)°, $Z = 2$), $[Cu\{(NMe_3)_2sar\}](ClO_4)_4$ (hexagonal $P\bar{6}2c$, a 8.689(2) Å, c 27.927(2) Å, $Z = 2$), and $[Zn\{(NMe_3)_2sar\}](ClO_4)_4$ (hexagonal, $P\bar{6}2c$, a 8.669(5) Å, c 27.998(5) Å, $Z = 2$) are reported. Visible–near-infrared absorption, circular dichroism, magnetic circular dichroism, and electron paramagnetic resonance spectroscopic studies reveal distorted CuN_6 chromophores. Trigonal distortions arise from steric requirements of the ligands, whereas tetragonal distortions result from Jahn–Teller coupling in the Cu(II) complexes. X-ray crystallographic studies of these copper(II) complexes revealed partially averaged ($[Cu\{(NH_3)_2sar\}]^{4+}$) and completely averaged ($[Cu\{(NMe_3)_2sar\}]^{4+}$) geometries as a result of both static disorder and dynamic processes throughout each lattice. Partial resolution of $[Cu\{(NMe_3)_2sar\}]^{4+}$ into its enantiomeric forms was achieved to give the first stable chiral molecule where Cu(II) is the stereogenic atom. In the absence of Jahn–Teller coupling characteristic of their Cu(II) relatives, the analogous Zn(II) complexes exhibited high-symmetry structures both in solution and in the solid state.

Introduction

The coordination chemistry of Cu(II) in an environment of six chemically equivalent ligands is notable in that the orbitally degenerate electronic ground state of the d^9 complex is unstable in an octahedral or trigonal ligand field, and lower symmetry geometries are invariably present. There are several reviews that deal with the relevant theory describing these systems,[3–5] but a brief overview of the salient features is appropriate here.

The Jahn–Teller effect manifests itself in this system by a coupling of the electronic ground state ^2E_g (O_h) with the normal vibrational mode of e_g symmetry. The vibrational mode can be considered as linear combinations of the Q_θ and Q_ϵ displacement coordinates (Figure 1). It can be seen that displacement along the Q_θ coordinate generates a tetragonally elongated or compressed geometry, whereas the Q_ϵ coordinate results in an orthorhombic distortion. Linear Jahn–Teller coupling lifts the orbital degeneracy of the ground state, and a so-called "Mexican hat" vibronic potential energy surface results. Looking at this surface, we see a continuous set of degenerate solutions along the valley of the surface (of radius R_{JT}, dashed line in Figure 1). Each point in this continuum at R_{JT} corresponds to a specific combination of the Q_θ and Q_ϵ (distorting) modes, where $Q_\theta = R_{JT}\cos\phi$ and $Q_\epsilon = R_{JT}\sin\phi$. The electronic component of the ground state wave function ψ

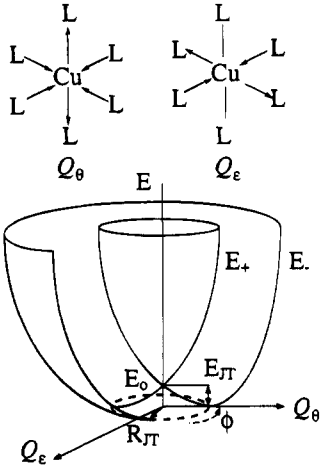

Figure 1. "Mexican hat" vibronic potential energy surface with Q_θ and Q_ϵ displacement coordinates for a Cu(II) complex in an octahedral ligand field.

then may be expressed as

$$\psi = d_{x^2-y^2}\cos(\phi/2) + d_{z^2}\sin(\phi/2) \quad (1)$$

Each combination defines a specific distortion away from octahedral symmetry, and each point on the "rim" of the Mexican hat is equally stabilized, relative to the octahedral CuL_6 species (energy E_o), by E_{JT}.

Although the linear Jahn–Teller term usually dominates, second and higher order Jahn–Teller interaction terms result in a small warping of the circular valley around the rim of the Mexican hat. Three minima and three saddle points characteristically result. The circular cross section of the warped

⊗ Abstract published in *Advance ACS Abstracts,* May 15, 1995.

(1) Australian National University.
(2) University of Western Australia.
(3) Gazo, J.; Bersuker, I. B.; Garaj, J.; Kabesova, M.; Kohout, J.; Langfelderova, H.; Melnik, M.; Serator, M.; Valach, F. *Coord. Chem. Revs.* **1976**, *19*, 253.
(4) Hathaway, B. J. *Struct. Bonding* **1984**, *57*, 55.
(5) Hitchman, M. A. *Comments Inorg. Chem.* **1994**, *15*, 197.

0020-1669/95/1334-3589$09.00/0

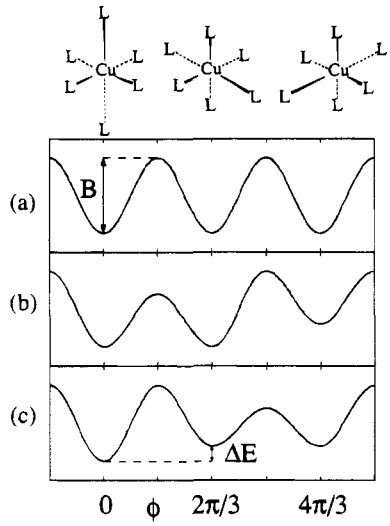

Figure 2. Circular cross sections of the minimum of the warped ground state potential energy surface (Figure 1): (a) octahedral or trigonal site symmetry; (b, c) general site symmetry.

potential energy surface as a function of the angle ϕ is shown in Figure 2a. The three degenerate minima will usually correspond to three tetragonally elongated geometries, and the three saddle points represent equivalent tetragonally compressed structures.

In the solid state, crystal packing effects often lower the C_{3v} symmetry of the surface. This may lead to the situation where only two minima remain degenerate. The remaining minimum may be higher (Figure 2b) or lower (Figure 2c) in energy. Of course all three minima may also be non-degenerate. It is important to appreciate that, in cases a and b, the crystallographically determined structure will be averaged. This may occur through static disorder of each degenerate orientation throughout the crystal or via dynamic interconversion between each geometry if the barrier heights (B) between the minima are sufficiently small relative to kT. Both static disorder and dynamic processes might be expected to impact on the thermal parameters of the CuL_6 core. Indeed this has been successfully modeled in selected cases via analysis of the anisotropic thermal parameters of both the CuL_6 core and a rigid-body analysis including the ligand framework.[6] However, it should be added that this method is not universally applicable, particularly in cases where significant conformational freedom in the ligand system is present.[7]

The coordination chemistry of the macrobicyclic amine sar (sar = 3,6,10,13,16,19-hexaazabicyclo[6.6.6]icosane) and its apically substituted relatives has revealed a strong tendency toward hexadentate coordination of these ligands to a wide variety of metal ions.[8] A structural feature of this chemistry has been the formation of complexes possessing essentially trigonal symmetry, with a slight compression along the C_3 axis. The degree of trigonal twist distortion has been shown to depend on the metal ion and to be particularly dependent on the specific conformation of the ligand.[9] Given that the trigonal ligand field offered by $(NH_2)_2$sar should be subject to Jahn–Teller distortions when coordinated to Cu(II), the structural and spectroscopic properties of the $[Cu\{(NR_3)_2sar\}]^{4+}$ ions (R = H, CH_3) have been probed. The permethylated analogue was investigated as an extension of previous work which found that methylation of the primary amines of $[Co\{(NH_3)_2sar\}]^{5+}$ resulted in some quite dramatic structural and spectroscopic changes.[10] It was of interest to see if similar variations in the Cu(II) chemistry would occur. As a supplement to this work, the isomorphous Zn(II) complexes were prepared and have been employed as diamagnetic hosts for their Cu(II) analogues in electron paramagnetic resonance (EPR) studies.

Experimental Section

Safety Note. Although we have experienced no problems with the compounds reported in this work, perchlorate salts are potentially explosive and should only be handled in small quantities, never heated in the solid state nor scraped away from sintered-glass frits.

Syntheses. All chemicals were AR grade. $(NH_2)_2sar{\cdot}5H_2O$ was synthesized as reported.[11]

(1,8-Diammonio-3,6,10,13,16,19-hexaazabicyclo[6.6.6]icosane) copper(II) Nitrate Hydrate, $[Cu\{(NH_3)_2sar\}](NO_3)_4{\cdot}H_2O$. To a solution of copper(II) nitrate trihydrate (0.83 g, 3.4 mmol) in 30 mL of water was added $(NH_2)_2sar{\cdot}5H_2O$ (1.40 g, 3.4 mmol). The solution was acidified to pH 4 with dilute HNO_3 and then evaporated on a steam bath until precipitation commenced. The blue product was collected by filtration, washed with ethanol and then diethyl ether, and dried in a vacuum desiccator (1.28 g, 60%). Anal. Calcd for $C_{14}H_{36}CuN_{12}O_{12}$: C, 26.77; H, 5.78; N, 26.76. Found: C, 26.5; H, 5.7; N, 26.9. Further crops were obtained from the filtrate. Crystals of $[Cu\{(NH_3)_2sar\}](NO_3)_4{\cdot}H_2O$ suitable for X-ray and spectroscopic analysis were grown by vapor diffusion of ethanol into a concentrated aqueous solution of $[Cu\{(NH_3)_2sar\}](NO_3)_4$.

(1,8-Diammonio-3,6,10,13,16,19-hexaazabicyclo[6.6.6]icosane)-zinc(II) Nitrate Hydrate, $[Zn\{(NH_3)_2sar\}](NO_3)_4{\cdot}H_2O$. This complex was prepared in a manner identical to that for its Cu(II) analogue, except $Zn(NO_3)_2{\cdot}6H_2O$ was used instead of $Cu(NO_3)_2{\cdot}3H_2O$. The yield of $[Zn\{(NH_3)_2sar\}](NO_3)_4$ was 70%. Anal. Calcd for $C_{14}H_{36}N_{12}O_{12}Zn$: C, 26.70; H, 5.76; N, 26.68. Found: C, 26.9; H, 5.9; N, 26.5. Crystals of $[Zn\{(NH_3)_2sar\}](NO_3)_4{\cdot}H_2O$ were grown by slow evaporation of an aqueous solution of $[Zn\{(NH_3)_2sar\}](NO_3)_4$. NMR ($D_2O$): ^1H (N-deuterated) δ 2.68, 3.36 (AA'BB', 12H), 3.06 and 3.48 (AB q, ^2J −13.4 Hz, 12H); ^{13}C δ 49.4 (CH_2), 51.6 (C_{tert}), 55.2 (CH_2).

(1,8-Bis(dimethylammonio)-3,6,10,13,16,19-hexaazabicyclo[6.6.6]-icosane)copper(II) Perchlorate Trihydrate, $[Cu\{(HNMe_2)_2sar\}](ClO4)_4{\cdot}3H_2O$. A solution of $[Cu\{(NH_3)_2sar\}](NO_3)_4$ (6.28 g, 10 mmol) in formic acid (100 mL, 98%) and aqueous formaldehyde (40 mL, 37%) was refluxed for 48 h. Unreacted formic acid was removed by evaporation at reduced pressure; the resulting residue was taken up in a minimum volume of hot water, and precipitation as a fine blue powder was achieved by addition of perchloric acid (2 mL, 70%). The product was collected by filtration, washed with ethanol and then diethyl ether, and dried in a vacuum desiccator (7.8g, 96%). Anal. Calcd for $C_{18}H_{50}Cl_4CuN_8O_{19}$: C, 24.34; H, 5.67; N, 12.62; Cl, 15.97. Found: C, 24.8; H, 5.7; N, 12.2; Cl, 15.8.

(1,8-Bis(trimethylammonio)-3,6,10,13,16,19-hexaazabicyclo[6.6.6]-icosane)copper(II) Perchlorate, $[Cu\{(NMe_3)_2sar\}](ClO_4)_4$. A solution of $[Cu\{(HNMe_2)_2sar\}](ClO_4)_4{\cdot}3H_2O$ (6.0 g, 7.2 mmol), dimethyl sulfate (6 mL, 63 mmol), and Na_2CO_3 (2.0 g, 19 mmol) in dimethylformamide (50 mL) was stirred for 24 h at 20 °C. The reaction mixture was diluted with water (100 mL) and the product precipitated as a fine blue powder upon addition of $HClO_4$ (5 mL, 70%). This was collected by filtration, washed with ethanol and then diethyl ether, and dried in a vacuum desiccator (5.6 g, 90%). Anal. Calcd for $C_{20}H_{48}Cl_4CuN_8O_{16}$: C, 27.87; H, 5.61; N, 13.00; Cl, 16.5. Found: C, 27.6; H, 5.4; N, 13.0; Cl, 16.28. Crystals of $[Cu\{(NMe_3)_2sar\}](ClO_4)_4$ suitable

(6) Ammeter, J. H.; Bürgi, H.-B.; Gamp, E.; Meyer-Sandrin, V.; Jensen, W. P. *Inorg. Chem.* **1979**, *18*, 733.
(7) Chaudhuri, P.; Oder, K.; Wieghardt, K.; Weiss, J.; Reedijk, J.; Hinrichs, W.; Wood, J.; Ozarowski, A.; Stratemeier, H.; Reinen, D. *Inorg. Chem.* **1986**, *25*, 2951.
(8) Sargeson, A. M. *Pure Appl. Chem.* **1986**, *58*, 1511 and references therein.
(9) Comba, P. *Inorg. Chem.* **1989**, *28*, 426.
(10) Bernhardt, P. V.; Bygott, A. M. T.; Geue, R. J.; Hendry, A. J.; Korybut-Daszkiewicz, B. R.; Lay, P. A.; Pladziewicz, J. R.; Sargeson, A. M.; Willis, A. C. *Inorg. Chem.* **1994**, *33*, 4553.
(11) Bottomley, G. A.; Clark, I. A.; Creaser, I. I.; Engelhardt, L. M.; Geue, R. J.; Hagen, K. S.; Harrowfield, J. M.; Lawrance, G. A.; Lay, P. A.; Sargeson, A. M.; See, A. J.; Skelton, B. W.; White, A. H.; Wilner, F. R. *Aust. J. Chem.* **1994**, *47*, 143.

Table 1. Crystal Data

	$[Cu\{(NMe_3)_2sar\}](ClO_4)_4$	$[Zn\{(NMe_3)_2sar\}](ClO_4)_4$	$[Cu\{(NH_3)_2sar\}](NO_3)_4 \cdot H_2O$	$[Zn\{(NH_3)_2sar\}](NO_3)_4 \cdot H_2O$
space group	$P\bar{6}2c$ (No. 190)	$P\bar{6}2c$ (No. 190)	$P2_1$ (No. 4)	$P2_1$ (No. 4)
formula	$C_{20}H_{48}Cl_4CuN_8O_{16}$	$C_{20}H_{48}Cl_4N_8O_{16}Zn$	$Cl_{14}H_{38}CuN_{12}O_{13}$	$Cl_{14}H_{38}N_{12}O_{13}Zn$
a, Å	8.689(2)	8.669(5)	12.311(3)	12.365.4
b, Å			12.338(4)	12.396(7)
c, Å	27.927(2)	27.998(5)	8.574(3)	8.587(4)
β, deg			93.91(3)	94.13(3)
V, Å^3	1825.8(7)	1822(2)	1299(1)	1313(1)
ϱ_{calcd}, g cm^{-3}	1.50	1.57	1.65	1.64
fw	862.01	863.84	646.08	647.91
Z	2	2	2	2
μ, cm^{-1}	40.6	10.1	9.3	10.5
temp, K	295	295	295	295
radiation; λ, Å	Cu; 1.541 78	Mo; 0.710 73	Mo; 0.710 73	Mo; 0.710 73
N	915	1081	3720	2438
N_o	614	816	3220	2185
$2\theta_{max}$, deg	120	50	60	50
$R(Fo)$, $R_w(F_o)$[a]	0.067, 0.077[b]	0.073, 0.077[b]	0.037, 0.040[c]	0.028, 0.034[c]

[a] $R(F_o) = \Sigma(||F_o| - |F_c||)/\Sigma|F_o|$; $R_w(F_o) = (\Sigma w(|F_o| - |F_c|)^2/\Sigma wF_o^2)^{1/2}$. [b] $w = (\sigma 2(F) + p(F)^2)^{-1}$. [c] Statistical weights; derivative of $\sigma^2(I) = \sigma^2(I_{diff}) + 0.0004\sigma^4(I_{diff})$.

for X-ray and spectroscopic studies were grown by slow evaporation of an aqueous solution of the complex.

1,8-Bis(trimethylammonio)-3,10-diazonia-6,13,16,19-tetraazabicyclo[6.6.6]icosane Perchlorate, $[(NMe_3)_2sarH_2](ClO_4)_4$. A solution of $[Cu\{(NMe_3)_2sar\}](ClO_4)_4$ (5 g, 5.8 mmol) in dilute HCl (200 mL, 0.25 M) was treated with zinc dust (5 g) and then stirred at 20 °C for 30 min. The colorless suspension was filtered, and the filtrate was sorbed onto a 15 × 4 cm column of Dowex 50W-X2 cation exchange resin (H^+-form, 200−400 mesh). The column was washed with 1 M HCl to remove Zn^{2+}, and the protonated ligand was then eluted with 3 M HCl. The hydrochloride salt was isolated by evaporating the eluate to dryness. Recrystallization was achieved by dissolving the residue in a minimum volume of hot water and precipitating by the addition of $HClO_4$ (3 mL, 70%). The solid was collected by filtration, washed with ethanol and then diethyl ether, and dried in a vacuum desiccator (3.85 g, 84%). Anal. Calcd for $C_{20}H_{50}Cl_4N_8O_{16}$: C, 30.01; H, 6.30; N, 13.00; Cl, 17.72. Found: C, 30.4; H, 6.4; N, 13.4; Cl, 17.6. NMR (D_2O): ^1H δ 3.11 (s, 12H), 3.64 (s, 12H), 3.27 (s, 18H); ^{13}C δ 49.3 (CH_2), 51.0 (CH_2), 51.3 (CH_3), 69.1 (C_{tert}).

(1,8-Bis(trimethylammonio)-3,6,10,13,16,19-hexaazabicyclo[6.6.6]-icosane)zinc(II) Perchlorate, $[Zn\{(NMe_3)_2sar\}](ClO_4)_4$. Zinc(II) chloride (0.20 g, 1.5 mmol) and $[(NMe_3)_2sarH_2](ClO_4)_4$ (1.20 g, 1.5 mmol) were dissolved in water (50 mL). Dilute aqueous NaOH was added to achieve a solution pH of 6, and the mixture was stirred at 60 °C for 1 h. Excess $NaClO_4 \cdot H_2O$ (1.6 g) was added, which resulted in immediate precipitation of the product. This was collected by filtration, washed with ethanol and then diethyl ether, and dried in a vacuum desiccator. Colorless crystals, suitable for X-ray work, were obtained by slow evaporation of an aqueous solution at ambient temperature (1.0 g, 77 %). Anal. Calcd for $C_{20}H_{48}Cl_4N_8O_{16}Zn$: C, 27.81; H, 5.60; N, 12.97; Cl, 16.42. Found: C, 27.3; H, 5.5; N, 12.8; Cl, 16.7. NMR: ^1H (D_2O, N-deuterated) δ 2.50 and 3.26 (AA′BB′ mult., 12H), 3.06 and 3.88 (AB q, $^2J = -13.2$ Hz, 12H), 3.14 (s, 18H). ^{13}C (DMSO-d_6) δ 48.2 (CH_2), 49.1 (CH_3), 49.5 (CH_2), 67.3 (C_{tert}).

Partial Resolution of $[Cu\{(NMe_3)_2sar\}](ClO_4)_4$. A solution of $[Cu\{(NMe_3)_2sar\}](ClO_4)_4$ (0.7 g) in water (300 mL) was sorbed onto a 1000 × 4 cm column of Sephadex C-25 cation exchange resin (Na^+-form). Elution with 0.25 M $Na_2[Sb_2((+)\text{-tartrate})_2]$ resulted in two incompletely separated bands. To the eluate of the first band was added an equal volume of 1 M $NaClO_4$ solution. Concentration of the solution to 100 mL resulted in precipitation of this fraction as the double salt $(+)_D$-$\{[Cu\{(NMe_3)_2sar\}](ClO_4)_4\}_2 \cdot Na_2[Sb_2((+)\text{tartrate})_2] \cdot H_2O$. This was collected by filtration, washed with ethanol and then diethyl ether, and dried in a vacuum desiccator (0.13 g, 13% of starting material). Anal. Calcd for $C_{24}H_{54}Cl_4CuN_8NaO_{23}Sb$: C, 24.58; H, 4.64; N, 9.55; Cl, 12.09. Found: C, 24.6; H, 4.4; N, 9.5; Cl, 13.0.

The second band from the resolution was diluted 8-fold with water, and rechromatographed on a small Sephadex C-25 column (10 × 3 cm) with 1 M NaCl being employed as the eluent. The product was precipitated by addition of an equal volume of 1 M $NaClO_4$ to the eluate. This was collected by filtration, washed with ethanol and then diethyl ether, and dried in a vacuum desiccator (0.37 g, 53% of starting material). Anal. Calcd for $C_{20}H_{48}Cl_4CuN_8O_{16}$: C, 27.87; H, 5.61; N, 13.00; Cl, 16.45. Found: C, 28.0; H, 6.5; N, 12.5; Cl, 16.5.

For EPR measurements, 1.0 g of $[Zn\{(NH_3)_2sar\}](NO_3)_4$ or $[Zn\{(NMe_3)_2sar\}](ClO_4)_4$ and 50 mg of the corresponding Cu(II) complex were dissolved in a minimum amount of hot water. On cooling, the pale blue product precipitated and was collected by filtration, washed with ethanol and then diethyl ether, and dried in a vacuum desiccator.

Instrumentation. NMR spectra were measured with a GEMINI 300 spectrometer at 300 (^1H) and 75 MHz (^{13}C), and all chemical shifts were referenced with 1,4-dioxane as an external calibrant (^{13}C δ 67.4 ppm, ^1H δ 3.74 ppm vs tetramethylsilane (TMS)) and are cited relative to TMS. EPR spectra were measured with a Varian V-4502 spectrometer employing a V-4561 34.99(1) GHz microwave bridge as calibrated by DPPH (g 2.0036). Samples were measured as either ca. 1 mM solutions in 1:2 DMF−H_2O or as 5% doped mixtures of the appropriate Cu(II) complexes in the isomorphous Zn(II) lattice. Spin Hamiltonian parameters were obtained by simulation of each spectrum with the program EPR50F.[12] Solution UV−vis−near-IR and (magnetic) circular dichroism spectra[13] and single-crystal polarized electronic spectra[14] were measured with equipment that has been described previously. Angular overlap model calculations were performed with the program CAMMAG.[15] Strain energy minimization calculations were performed with the program MOMEC87.[16] Additional force field parameters were included for the present study: r_o (Cu−N_{eq}) 2.03 Å; r_o (Cu−N_{ax}) 2.36 Å. All other parameters have been reported previously.[17] Starting coordinates were taken from the appropriate crystal structure.

X-ray Crystal Structure Analyses. Unique 295 K diffractometer data sets were measured (2Θ/Θ scan mode; monochromatic Kα radiation) yielding N independent reflections, N_o with $I > 3\sigma(I)$ being considered "observed" and used in the full-matrix refinement (anisotropic thermal parameter refinement for the non-H atoms except for disordered atoms with partial occupancies; absorption-corrected data). Conventional residuals R and R_w on $|F|$ are quoted at convergence. Neutral atom complex scattering factors were employed. Pertinent crystal data are given in Table 1, and the atomic nomenclature is defined

(12) Martinelli, R. A.; Hanson, G. R.; Thompson, J. S.; Holmquist, B.; Pilbrow, J. R.; Auld, D. S.; Vallee, B. L. *Biochemistry* **1989**, *28*, 2251.
(13) Krausz, E.; Ludi, A. *Inorg. Chem.* **1985**, *24*, 939.
(14) Krausz, E. *Aust. J. Chem.* **1993**, *46*, 1041.
(15) Cruse, D. A.; Davies, J. E.; Gerloch, M.; Harding, J. H.; Mackey, D. J.; McMeeking, R. F. CAMMAG, a FORTRAN program. Univeristy of Cambridge, U. K., 1991.
(16) Hambley, T. W. MOMEC87, a Program for Strain Energy Minimization. University of Sydney, Australia, 1987.
(17) Bernhardt, P. V.; Comba, P. *Inorg. Chem.* **1992**, *31*, 2638.

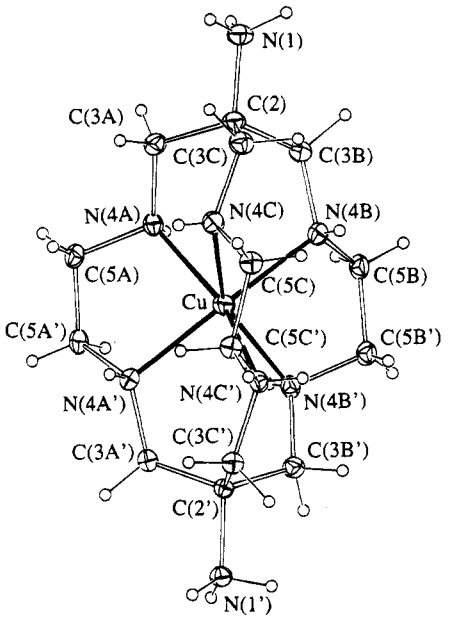

Figure 3. ORTEP drawing of the $[Cu\{(NH_3)_2sar\}]^{4+}$ cation. 20% thermal ellipsoids are shown for non-H atoms; H atoms have arbitrary radii of 0.1 Å.

in Figures 3 and 4. Individual variations and abnormal features are as follows.

$[M\{(NMe_3)_2sar\}](ClO_4)_4$. Empirical ($\Psi$-scan) absorption corrections were applied. The model adopted in space group $P\bar{6}2c$ comprised superimposed enantiomeric cations defined by pairs of coordinated N atom sites N(4, 4′). Perchlorate ions were disordered about their 3-fold axes. For perchlorate 1, no O atoms lay on the 3-axis and all were refined with site occupancy $^1/_3$. In perchlorate 2, O(2A) was located on the 3-axis, whereas the other O atoms occupied disordered pairs of sites O(2B, 2B′), refined with complementary occupancies. H atoms were included in the calculations with C−H and N−H fixed at 0.97 and 0.91 Å, respectively. Calculations were performed with SHELX-76.[18] Atomic scattering factors,[19] anomalous dispersion effects,[20] values of $\Delta f'$ and f'' [21] and the mass attenuation coefficients[22] were taken from the literature.

$[M\{(NH_3)_2sar\}](NO_3)_4{\cdot}H_2O$. Gaussian absorption corrections were applied; H atoms were not located for the water molecule, but the remainder were refined in (x, y, z, U_{iso}). Residuals quoted are for the chiralities presented, established by refinement for the specimens used. Computation used the X-RAY[23] and XTAL 3.2[24] systems. The setting adopted for both structures follows that previously defined for the isomorphous Mn(II) analogue.[25]

Results

Complexation of $(NH_2)_2sar$ with the labile metal ions Cu(II) and Zn(II) was straightforward, and their complexes were crystallized readily as the diprotonated tetranitrate hydrate salts. Successive methylation of the primary amines on $[Cu\{(NH_3)_2sar\}]^{4+}$ to yield $[Cu\{(HNMe_2)_2sar\}]^{4+}$ and ultimately $[Cu\{(NMe_3)_2sar\}]^{4+}$ was performed in a manner identical to that reported for the analogous Co(III) chemistry.[10] Demetalation of $[Cu\{(NMe_3)_2sar\}]^{4+}$ was achieved by reduction with zinc in dilute acid, and precipitation of the protonated ligand as either the chloride or the perchlorate salt occurred readily. Recomplexation of $[(NMe_3)_2sar]^{2+}$ with Zn(II) was accomplished in a manner similar to that for the unmethylated parent. The Cu(II) and Zn(II) complexes of $[(NMe_3)_2sar]^{2+}$ were crystallized as their tetraperchlorate salts, which were relatively poorly soluble in water.

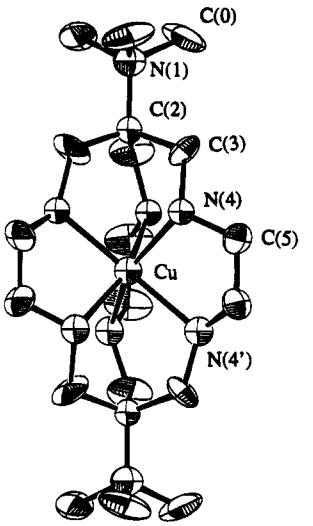

Figure 4. ORTEP drawing of the $[Cu\{(NMe_3)_2sar\}]^{4+}$ cation (H atoms omitted for clarity).

X-ray crystal structural analyses of $[M\{(NH_3)_2sar\}](NO_3)_4{\cdot}H_2O$ (M = Cu, Zn) were undertaken. The structure of $[Cu\{(NH_3)_2sar\}](NO_3)_4{\cdot}H_2O$ has the complex cation, four anions, and a water molecule each on general sites. This same lattice has been identified for $[M\{(NH_3)_2sar\}]^{4+}$ complexes of other divalent metal ions.[11,25-27] A plot of the cation $[Cu\{(NH_3)_2sar\}]^{4+}$ is shown in Figure 3 where hexadentate coordination of the ligand and a *lel* conformation of each five-membered chelate ring is defined. The *lel* and *ob* nomenclature refers to the orientation of the C−C bond of the chelate ring being parallel and oblique to the (pseudo) C_3 axis of the complex, respectively.) Inspection of Table 2 reveals that, despite the symmetry of the hexadentate coordinated ligand, the six Cu−N bonds are not equivalent. Instead, one pair of trans Cu−N bonds (2.251(3), 2.298(4) Å) is significantly longer than the remaining four (2.088(3)-2.148(7) Å). An additional distortion is superimposed, defined by the pseudo trigonal twist angle φ of 30-(4)°, where $\varphi = 60°$ for octahedral symmetry and 0° for trigonal prismatic geometry. (Strictly speaking, the trigonal twist angle is only appropriate for molecules possessing trigonal symmetry. The molecule has lost its 3-fold symmetry as a result of tetragonal distortion.) There are several hydrogen bonds between the ammonium groups and the water and nitrate O atoms, in addition to contacts between the coordinated amines N(4A) and N(4C) and nitrate O atoms. This array has been described in detail for the Mn(II) analogue.[25]

The crystallographic analysis of $[Zn\{(NH_3)_2sar\}](NO_3)_4{\cdot}H_2O$ revealed this complex to be isostructural with the Cu(II) analogue. Interestingly, although the variations in the Zn−N bond lengths are relatively minor, the longest bond (Table 2) is

(18) Sheldrick, G. M. SHELX-76: A Program for Crystal Structure Determination. University of Cambridge, U.K., 1976.
(19) Cromer, D. T.; Waber, J. T. *International Tables for X-ray Crystallography*; The Kynoch Press: Birmingham, U.K., 1974; Vol. IV.
(20) Ibers, J. A.; Hamilton, W. C. *Acta Crystallogr.* **1964**, *17*, 781.
(21) Creagh, D. C.; McAuley, W. J. *International Tables for Crystallography*; Kluwer Academic Publishers: Boston, MA, 1992; Vol. C, p 219.
(22) Creagh, D. C.; Hubbell, J. H. *International Tables for Crystallography*; Kluwer Academic Publishers: Boston, MA, 1992; p 200.
(23) Stewart, J. M. The X-RAY System, Computer Science Center, University of Maryland: 1976.
(24) Hall, S. R.; Flack, H. D.; Stewart, J. M. The XTAL 3.2 User's Manual. Universities of Western Australia, Geneva, and Maryland, 1992.
(25) Creaser, I. I.; Engelhardt, L. M.; Harrowfield, J. M.; Sargeson, A. M.; Skelton, B. W.; White, A. H. *Aust. J. Chem.* **1993**, *46*, 465.
(26) Clark, I. J.; Creaser, I. I.; Engelhardt, L. M.; Harrowfield, J. M.; Krausz, E. R.; Moran, G. M.; Sargeson, A. M.; White, A. H. *Aust. J. Chem.* **1993**, *46*, 111.
(27) Comba, P.; Sargeson, A. M.; Engelhardt, L. M.; Harrowfield, J. M.; White, A. H.; Horn, E.; Snow, M. R. *Inorg. Chem.* **1985**, *24*, 2325.

Table 2. Selected Bond Lengths (Å) and Angles (deg)

	$[Cu\{(NH_3)_2sar\}]^{4+}$	$[Zn\{(NH_3)_2sar\}]^{4+}$	$[Cu\{(NMe_3)_2sar\}]^{4+}$ [a]	$[Zn\{(NMe_3)_2sar\}]^{4+}$ [a]
M−N(4A)	2.094(3)	2.176(4)	2.17(1)	2.19(1)
M−N(4A′)	2.088(3)	2.190(4)	2.16(2)	2.19(1)
M−N(4B)	2.127(3)	2.189(4)		
M−N(4B′)	2.251(3)	2.198(4)		
M−N(4C)	2.298(4)	2.216(4)		
M−N(4C′)	2.148(3)	2.174(3)		
N(4A)−M−N(4B)	87.3(1)	86.1(1)	85.6(6)	85.0(4)
N(4A)−M−N(4C)	84.7(1)	84.6(1)		
N(4A)−M−N(4A′)	83.7(1)	80.7(1)	81.9(6)	82.3(4)
N(4A)−M−N(4B′)	116.2(1)	113.5(1)	113.1(6)	114.0(4)
N(4A)−M−N(4C′)	156.4(1)	154.7(1)	156.5(6)	156.0(4)
N(4B)−M−N(4C)	84.0(1)	85.7(1)		
N(4B)−M−N(4A′)	158.6(1)	155.5(1)		
N(4B)−M−N(4B′)	79.3(1)	80.4(1)		
N(4B)−M−N(4C′)	1088.4(1)	113.3(1)		
N(4C)−M−N(4A′)	114.4(1)	113.2(1)		
N(4C)−M−N(4B′)	152.2(1)	156.0(1)		
N(4C)−M−N(4C′)	79.3(1)	81.1(1)		
N(4A′)−M−N(4B′)	87.3(1)	86.1(1)	84.7(6)	84.6(4)
N(4A′)−M−N(4C′)	86.7(1)	86.0(1)		
N(4B′)−M−N(4C′)	84.7(1)	86.7(1)		

[a] In these structures, the A(′), B(′), and C(′) nomenclature refers to the cofacial symmetry-related N atoms.

coincident with the longest Cu−N bond found in $[Cu\{(NH_3)_2sar\}]^{4+}$, which is indicative of relaxation of the longest M−N bond in the latter being assisted by preexisting lattice forces. For this reason, the three minima in the rim of the Mexican hat potential energy surface are no longer degenerate (Figure 2c). Thermal motion in the Cu(II) complex lattice is somewhat higher than that observed in the lattice of the Zn(II) analogue, but without conspicuous association with any particular atom or set of atoms within the cations.

The X-ray structural analysis of $[Cu\{(NMe_3)_2sar\}](ClO_4)_4$ models the complex cation as being located about a $\bar{6}$ site in space group $P\bar{6}2c$, with two perchlorate anions on 3-fold axes. The model used for solution of the structure defined a disordered array of the Λ and Δ enantiomers of the cation throughout the lattice (see Experimental Section), and there was no significant difference between the two independent Cu−N bond lengths. A view of one of the enantiomers is shown in Figure 4. The conformation of the ligand was the same as that found in the structure of $[Cu\{(NH_3)_2sar\}](NO_3)_4{\cdot}H_2O$, and a trigonal twist distortion of $\varphi = 29.7(1)°$ was determined. The crystallographic analysis of $[Zn\{(NMe_3)_2sar\}](ClO_4)_4$ found this complex to be isostructural with its Cu(II) relative. The two independent Zn−N bond lengths (Table 2) did not differ significantly from those found in the structure of $[Zn\{(NH_3)_2sar\}](NO_3)_4{\cdot}H_2O$, and the trigonal twist angle ($\varphi = 28.9(1)°$) was also similar.

In neutral aqueous solution, the physical properties of corresponding methylated and unmethylated cage complexes were rather similar. The N-deuterated ^1H NMR spectra of $[Zn(sar)]^{2+}$, $[Zn\{(NH_3)_2sar\}]^{4+}$, and $[Zn\{(NMe_3)_2sar\}]^{4+}$ in D_2O exhibited similar AA′BB′ and AB (ABX in the case of $[Zn(sar)]^{2+}$) spin coupling patterns corresponding to their five-membered chelate rings and cap methylene groups, respectively. The spectrum of $[Zn\{(NMe_3)_2sar\}]^{4+}$ displayed an additional singlet due to the trimethylammonio groups. Similarly, the solution visible electronic spectra of $[Cu(sar)]^{2+}$, $[Cu\{(NH_3)_2sar\}]^{4+}$, and $[Cu\{(NMe_3)_2sar\}]^{4+}$ in neutral aqueous solution were essentially the same, indicating that the presence of the two apical amine/ammonio (pK_{a1} 6.03(2), pK_{a2} 5.24(2), μ 0.1 M, 25 °C) or trimethylammonio groups has little influence on the CuN_6 chromophore. These observations are in contrast with those for the corresponding Co(III) complexes, where marked spectroscopic amd structural variations were observed upon going from either $[Co(sar)]^{3+}$ or $[Co\{(NH_3)_2sar\}]^{5+}$ to $[Co\{(NMe_3)_2sar\}]^{5+}$.[10]

However, it was found that the tetrapositively charged, ammonium-substituted complexes exhibited remarkable stability in acid solution relative to their $[M(sar)]^{2+}$ analogues. For example, the solution visible maximum of $[Cu(sar)]^{2+}$ shifted immediately upon acidification ($[H^+]$ *ca.* 0.1 M) from 15 200 to 19 400 cm^{-1} to afford a violet solution. An X-ray crystallographic analysis has found that this violet species is $[Cu(sarH_2)]^{4+}$ where the ligand coordinates as a tetradentate, and a pair of *cis* amines are protonated.[28] By contrast, no changes in the spectra of $[Cu\{(NH_3)_2sar\}]^{4+}$ and $[Cu\{(NMe_3)_2sar\}]^{4+}$ in 2 M HCl, relative to their spectra in neutral solution, were observed over a period of several months. As expected from the Irving−Williams series, the $[Zn(sar)]^{2+}$ ion was less resistant to acid dissociation than its Cu(II) analogue. Complete and rapid dissociation of $[Zn(sar)]^{2+}$ occurred in 2 M DCl as shown by ^1H NMR spectroscopy, where the resulting solution gave rise to a spectrum identical to that of the protonated free ligand, whereas $[Zn\{(NH_3)_2sar\}]^{4+}$ and $[Zn\{(NMe_3)_2sar\}]^{4+}$ exhibited similar spectra in both neutral and acidic media. A comprehensive kinetic and structural analysis of the acid-catalyzed dissociation of $[Cu(sar)]^{2+}$ and $[Zn(sar)]^{2+}$ will be published separately.[28]

The 40 K Q-band (35 GHz) EPR spectra of $[Cu\{(NH_3)_2sar\}](NO_3)_4$ and $[Cu\{(NMe_3)_2sar\}](ClO_4)_4$, as dilute frozen H_2O−DMF solutions, were virtually identical. Three distinct g values were obtained from simulation of the experimental spectra: g_z 2.22(1) (A_z = 130(2) G), g_y = 2.12(1) (A_y = 55(5) G), and g_x = 2.07(1) (A_x =15(5) G). These data are consistent with a $d_{x^2-y^2}$ ground state, arising from a tetragonally elongated CuN_6 chromophore ($g_z \gg g_y, g_x$) with an additional orthorhombic distortion ($g_y \neq g_x$). The 293 K solution spectrum of $[Cu\{(NMe_3)_2sar\}]^{4+}$ yielded isotropic spin Hamiltonian parameters g_{iso} = 2.13(1) and A_{iso} = 68(2) G (consistent with $g_{iso} = (g_x + g_y + g_z)/3$ and $A_{iso} = (A_x + A_y + A_z/3)$. A broad signal with unresolved hyperfine coupling centered at g_{iso} = 2.12(1) was observed for the 293 K spectrum of $[Cu\{(NH_3)_2sar\}]^{4+}$.

The polycrystalline EPR spectra of $[Cu\{(NMe_3)_2sar\}](ClO_4)_4$ doped into the isomorphous $[Zn\{(NMe_3)_2sar\}](ClO_4)_4$ lattice, as a function of temperature, are shown in Figure 5. Between

(28) Grondahl, L.; Sargeson, A. M.; White, A. H. Unpublished results.

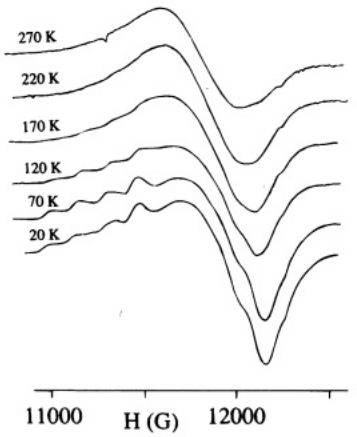

Figure 5. Q-Band EPR spectra of 5% $[Cu\{(NMe_3)_2sar\}](ClO_4)_4$ doped in $[Zn\{(NMe_3)_2sar\}](ClO_4)_4$ as a function of temperature.

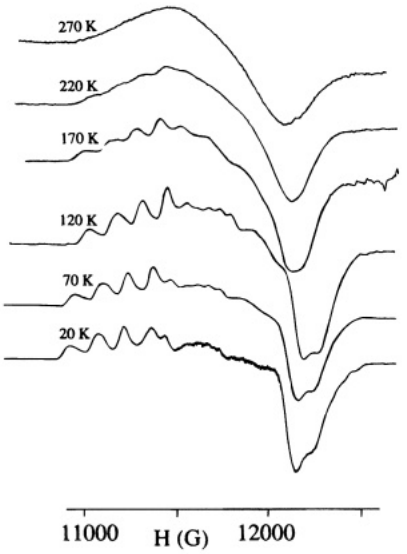

Figure 6. Q-Band EPR spectra of 5% $[Cu\{(NH_3)_2sar\}](NO_3)_4$ doped in $[Zn\{(NH_3)_2sar\}](NO_3)_4$ as a function of temperature.

20 and 120 K, the spectra were invariant and exhibited g values similar to those obtained from the frozen solution spectrum, although the $A_{||}$ value was somewhat greater in the solid state spectrum (160(2) G). Above 120 K, no hyperfine resonances were resolved, which ultimately resulted in an essentially isotropic 293 K spectrum. The spectrum of $[Cu\{(NH_3)_2sar\}](NO_3)_4 \cdot H_2O$ doped into the isomorphous $[Zn\{(NH_3)_2sar\}](NO_3)_4 \cdot H_2O$ lattice (Figure 6) exhibited behavior quite different from that of its methylated relative. As the temperature increased from 20 to 220 K, g_z decreased continuously from *ca.* 2.24 to 2.21, A_z decreased from *ca.* 150 to 120 G, and g_x increased from *ca.* 2.05 until it merged with the remaining resonances of the spectrum. Resonances around $g_y = 2.14$ appeared between 70 and 170 K and then merged with the remainder of the spectrum with increasing temperature.

The electronic spectra of $[Cu\{(NH_3)_2sar\}]^{4+}$ and $[Cu\{(NMe_3)_2sar\}]^{4+}$ in D_2O solution were rather similar. The spectrum of $[Cu\{(NH_3)_2sar\}]^{4+}$ exhibited maxima at 8500 cm^{-1} (ϵ 59 M^{-1} cm^{-1}, $d_{z^2} \leftarrow d_{x^2-y^2}$) and 15 200 cm^{-1} (ϵ 140 M^{-1} cm^{-1}, $d_{xy}, d_{yz}, d_{xz} \leftarrow d_{x^2-y^2}$), whereas the spectrum of $[Cu\{(NMe_3)_2sar\}]^{4+}$ revealed transitions at 8730 cm^{-1} (ϵ 64 M^{-1} cm^{-1}) and 15 400 cm^{-1} (ϵ 150 M^{-1} cm^{-1}), respectively. The existence of the near-IR maximum in each spectrum provides evidence that the geometries of the two CuN_6 chromophores are tetragonally distorted, although the X-ray crystal structure analysis of $[Cu\{(NMe_3)_2sar\}]^{4+}$ did not resolve this distortion. The near-IR maximum

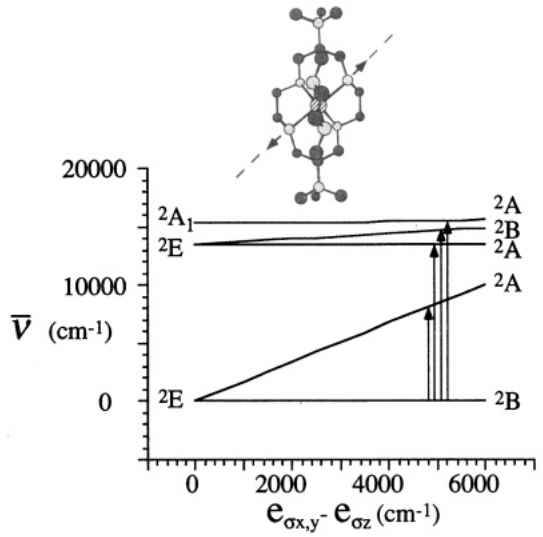

Figure 7. AOM correlation diagram for $[Cu\{(NR_3)_2sar\}]^{4+}$ (R = H, CH_3) as a function of a tetragonal elongation along the direction shown by the arrows. The parameters $e_{\sigma x}$, $e_{\sigma y}$, and $e_{\sigma z}$ refer to the three independent Cu−N bonds in C_2 symmetry. In this case $e_{\sigma x} = e_{\sigma y}$ and $e_{\sigma z}$ corresponds to the longest Cu−N bond.

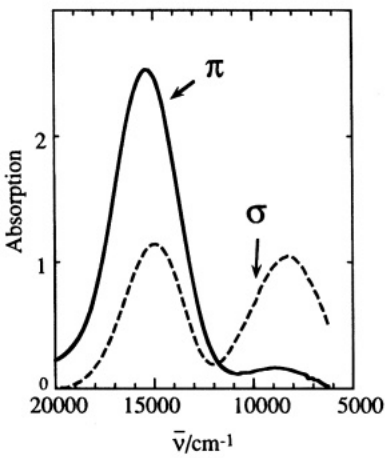

Figure 8. Polarized absorption spectra of a 50 μm × 80 μm, *ca.* 35 μm thick crystal of $[Cu\{(NMe_3)_2sar\}](ClO_4)_4$ at 295 K.

arises from a transition between the two components of ^2E_g (O_h) parentage which split as a result of the tetragonal, but not the trigonal twist, distortion. (Figure 7). Splitting of the $^2T_{2g}$ (O_h) state in the lower symmetry ligand field was less conspicuous, with the components of this envelope lying too close in energy to be resolved in the solution absorption spectrum. However, resolution of this group of transitions into two components was achieved in the polarized single-crystal absorption spectra and the solution circular dichroism spectrum of $[Cu\{(NMe_3)_2sar\}]^{4+}$ (see below).

The 298 K single-crystal polarized electronic spectra of $[Cu\{(NMe_3)_2sar\}](ClO_4)_4$ where the electric vector is perpendicular (σ) and parallel (π) to the crystallographic 3-fold (c) axis are shown in Figure 8. Two maxima were apparent in each spectrum. The lower energy band, which is strongly σ polarized, appears near 8500 cm^{-1}, while the higher energy feature, near 15 200 cm^{-1}, is somewhat more intense in the π spectrum than in the σ spectrum. A simulated isotropic absorption spectrum, obtained by taking the combination of polarized spectra in Figure 8 of $(2\sigma + \pi)/3$, was compared to the solution spectrum of the chromophore. The agreement, allowing for a blue shift of ca. 400 cm^{-1} in solution, was satisfactory. This provides evidence that the chromophores in both crystalline and solution environments are similar.

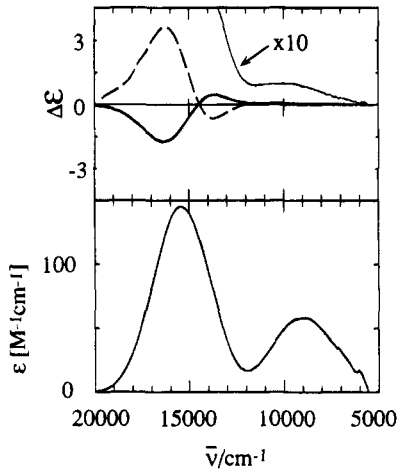

Figure 9. Solution absorption spectrum (lower panel) and CD spectra (upper panel) of $[Cu\{(NMe_3)_2sar\}]^{4+}$ in D_2O at 295 K. Spectra are baseline corrected for solvent absorption.

The polarization properties of $[Cu\{(NMe_3)_2sar\}](ClO_4)_4$ are similar to those of $[Cu(en)_3](SO_4)$ (en = ethane-1,2-diamine),[29] which also has crystallographically imposed trigonal site symmetry at room temperature.[30] The observation of a strong (>5: 1) polarization of the near-IR band (Figure 8) of $[Cu\{(NMe_3)_2sar\}](ClO_4)_4$ along what is a pseudo 3-fold axis of the chromophore is surprising, given that a dominant tetragonal elongation is present in each chromophore (approximately 55° to the c axis), and polarizations might be expected to be more strongly related to these tetragonal molecular directions. This point will be taken up further in the discussion.

Given that $[Cu\{(NMe_3)_2sar\}]^{4+}$ displayed such resistance to dissociation under acidic conditions, resolution into its enantiomeric Λ and Δ forms by cation exchange chromatography was attempted using the chiral eluent sodium antimony (+)-tartrate. Partial resolution was achieved as shown by the circular dichroism (CD) spectra of the two isolated fractions (Figure 9). Extrema in the CD spectra occur at ca. 13 700 cm^{-1} and at *ca.* 16 400 cm^{-1}. A weak, broad CD maximum was observed at *ca.* 10 000 cm^{-1}. The CD provides evidence that the broad visible maximum seen in absorption is composed of at least two transitions, exhibiting circular dichroism of opposite sign. The energy positions of CD extrema do not provide values of the transition energies, due to the degree of overlap of the two bands. The solution CD and absorption spectra were simultaneously fitted, using two Gaussian line shapes and a global least-squares-fitting procedure. This allowed an estimation of the position the two components as 14 500 and 15 200 cm^{-1}. The corresponding Gaussian widths at half-height were 2600 and 3600 cm^{-1} respectively. The CD and absorption spectra were quantitatively reproduced.

The measured $\Delta\epsilon$ values for the CD maxima of the two fractions were not equal and opposite. This indicates that at least one fraction, and probably both, were not fully resolved. The change in optical activity of one of the partially resolved fractions of $[Cu\{(NMe_3)_2sar\}]^{4+}$ as a function of time and pH was monitored by spectropolarimetry at 589 nm. The observed first-order rate constants (s^{-1}) were 9×10^{-5} (pH 1.5), 8×10^{-5} (pH 6.0), 4×10^{-5} (pH 7.8), and 1×10^{-4} (pH 9.2). In each case, the final product still exhibited optical activity, which indicated that racemization was not occurring during the experiment, only mutarotation.

The single-crystal polarized vis-near-IR absorption spectra of a small rectangular plate of $[Cu\{(NH_3)_2sar\}](NO_3)_4{\cdot}H_2O$ at

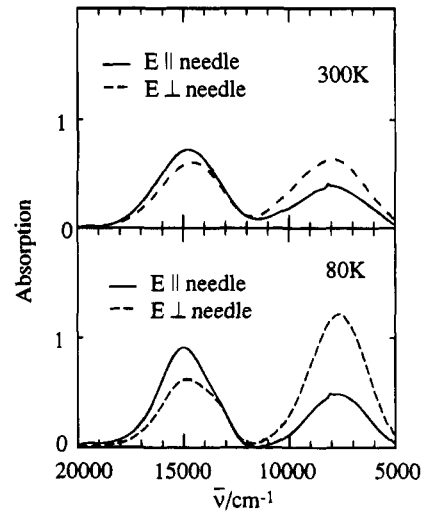

Figure 10. Polarized absorption spectra of a *ca.* 200 μm × 300 μm, *ca.* 30 mm thick crystal of $[Cu\{(NH_3)_2sar\}](NO_3)_4{\cdot}H_2O$ at 300 and 80 K.

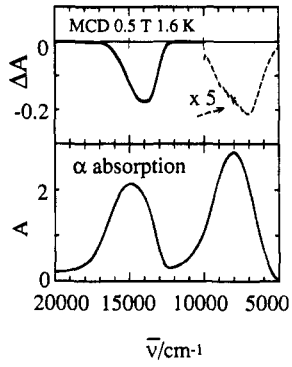

Figure 11. Axial absorption spectrum (lower panel) and MCD spectrum (upper panel) of a crystal plate of $[Cu\{(NMe_3)_2sar\}](ClO_4)_4$ of *ca.* 900 μm o.d. and *ca.* 110 μm thickness at 1.6 K.

293 and 77 K are shown in Figure 10. It was not possible to perform the spectroscopic measurements with the same crystal used for the X-ray structural determination of $[Cu\{(NH_3)_2sar\}](NO_3)_4{\cdot}H_2O$. Nevertheless, the polarization properties of the crystal were most consistent with an orientation of the plate such that the incident light was perpendicular to the (001) crystal face (see Discussion). Asymmetry in the high-energy band is clearly revealed in the polarized spectra. Fitting procedures analogous to those used for the solution CD spectra were used to gauge the positions of the two components of the visible envelope (at 80 K) as 14 600 and 15 200 cm^{-1}. Again the lower energy feature is considerably narrower (2300 cm^{-1}) than that at higher energy (3900 cm^{-1}). The energy separation (600 cm^{-1}) compares well to that obtained from the 293 K solution CD analysis of $[Cu\{(NMe_3)_2sar\}]^{4+}$ (1000 cm^{-1}). The single-crystal polarized spectra of $[Cu\{(NH_3)_2sar\}](NO_3)_4{\cdot}H_2O$ show a rather strong temperature dependence.

The magnetic circular dichroism (MCD) spectrum of a thin crystal of $[Cu\{(NMe_3)_2sar\}](ClO_4)_4$ which grew with its c axis perpendicular to its large face is shown in Figure 11. Intense temperature-dependent (C term) MCD signals were observed. For measurements at 1.6 K the magnetic field used was reduced to 0.5 T to limit ΔA values to less than 0.2. Measurements at these low fields ensured that values of ΔA obtained were within the linear regime. Simultaneously presented in Figure 11 is the α-polarized absorption spectrum, which is identical to the σ-polarized spectrum for electric dipole transition processes.

The low-energy band has a relatively weak MCD, and its shape does not follow that of the absorption spectrum. Larger

(29) Bertini, I.; Gatteschi, D. *Inorg. Nucl. Chem. Lett.* **1972**, *8*, 207.
(30) Cullen, D. L.; Lingafelter, E. C. *Inorg. Chem.* **1970**, *9*, 1858.

Table 3. Spectral Properties of (Hexaamine)copper(II) Complexes

	d_o, Å	$\bar{\nu}_{max}$, cm^{-1}	g_{iso}	g_x	g_y	g_z
$[Cu(tach)_2]^{2+}$	2.17[a]	8800, 15 750	2.12	2.05	2.05	2.25
$[Cu(taci)_2]^{2+}$	2.17[b]	15 730	2.12	2.055	2.055	2.262
$[Cu(en)_3]^{2+}$	2.15[c]	8700, 15 700[d]	2.12[e]	2.08	2.08	2.25
$[Cu(tacn)_2]^{2+}$	2.15[f]	7200, 16 300	2.11	2.05	2.05	2.22
$[Cu\{(NH_3)_2sar\}]^{4+}$	2.17[g]	8500, 15 200	2.13	2.07	2.11	2.22
$[Cu\{(NMe_3)_2sar\}]^{4+}$	2.16[g]	8730, 14 500, 15 200	2.13	2.07	2.11	2.22
$[Cu(pn)_3]^{2+}$	2.16[h]	15 500				
$[Cu(Me_5\text{-}N_6\text{-tricosane})]^{2+}$	2.18[i]	16 400	2.11	2.06	2.06	2.25

[a] Reference 6. [b] Hegetschweiler, K.; Gramlich, V.; Ghisletta, M.; Samaras, H. *Inorg. Chem.* **1992**, *31*, 2341. [c] Reference 30; en = ethane-1,2-diamine. [d] Reference 29. [e] Reference 36. [f] Reference 7. [g] This work. [h] Okamoto, T.; Matsumoto, K.; Kuroya, H. *Bull. Chem. Soc. Jpn.* **1970**, *43*, 1915; pn = propane-1,2-diamine. [i] Ralph, S. F.; Sargeson, A. M.; White, A. H. Unpublished results.

values of $\Delta A/A$ are evident on the low-energy side of the band, and this immediately indicates the involvement of vibronic inducing (Herzberg–Teller) modes in the system.[31] When only totally symmetric modes are involved in transition processes, *C* terms have the same line shape as absorption. Attempts to simultaneously fit absorption and MCD spectra in the visible region to two Gaussians, as achieved for the CD and polarized absorption spectra (above) failed. This is again evidence that vibronic inducing processes are also responsible for at least some of the intensity in the visible region.

Discussion

Studies of Cu(II) complexes in nominally cubic or trigonal ligand fields have highlighted some interesting spectroscopic and structural results. Although there are several examples where X-ray crystallographic investigations have defined octahedral[32] or trigonal[30,33] site symmetry of the CuL_6 core, vis-near-IR and EPR spectroscopic studies have invariably indicated that the underlying symmetry of the complex was much lower.[34–36] That is, the crystallographically determined structure was merely a weighted average which arose from static disorder ($B > kT$) or dynamic averaging ($B < kT$) of the three distorted geometries depicted in Figure 2, or both.

It has been found that despite structural variations in the type of ligand, e.g. primary or secondary amine, macrocyclic or acyclic ligand, etc., the spectroscopic constants ($\bar{\nu}_{max}$, $g_{x,y,z}$, $A_{x,y,z}$) and the average Cu–N bond length (d_o) for a range of (hexaamine)copper(II) complexes are rather similar (Table 3). The vis-near-IR spectroscopic data reflect the underlying tetragonally distorted geometry of each chromophore because electronic transitions occur over a sufficiently short time scale ($\sim 10^{-15}$ s) that the nuclei may be considered to be at their respective extrema defined by the molecular vibration. The fact that these data are essentially invariant despite the diversity of the ligands indicates that the ground and excited state potential energy surfaces are quite resistant to the effects of intramolecular strain. This behavior is quite uncommon, as differences of as much as 0.1 Å in the average M–N bond lengths and 4000 cm^{-1} in the electronic maxima are typical for the same ligand systems listed in Table 3 complexed with other transition metal ions.

Solution Properties. The resistance of both $[M\{(NH_3)_2sar\}]^{4+}$ and $[M\{(NMe_3)_2sar\}]^{4+}$ (M = Cu, Zn) to acid-catalyzed dissociation, and racemization in the case of the latter Cu(II) complex, relative to their $[M(sar)]^{2+}$ parent complexes is a consequence of their higher charge. The high charge results in a reduced affinity of the tetrapositively charged complex for an incoming proton. Therefore, when protonated, the putative $[M\{(NH_3)_2sarH\}]^{5+}$ and $[M\{(NMe_3)_2sarH\}]^{5+}$ complexes are not sufficiently long-lived to allow conformational rearrangement whereby the protonated amine is displaced from the metal center.

The stability of the $[Cu\{(NMe_3)_2sar\}]^{4+}$ ion permitted its partial resolution into its Λ and Δ enantiomers, which still exhibit optical activity after several months in aqueous solution. To our knowledge, the resolution and solution CD of a Cu(II) complex of an achiral ligand have not been reported before. The lability of these systems generally dictates that racemization occurs too rapidly to allow resolution other than by precipitation as racemic mixtures of enantiomorphic crystals. In any case, these conglomerates undergo racemization immediately upon dissolution, so CD measurements have been restricted to the solid state.[37]

It was found that the solution optical rotation or the intensity of the CD maxima of a partially resolved fraction of $[Cu\{(NMe_3)_2sar\}]^{4+}$ decreased with a pH independent ($1.5 < pH < 9.2$) first-order rate constant of $8(2) \times 10^{-5}$ s^{-1} ($t_{1/2} \approx 5$ h). However, the final product of this process still exhibited optical activity, i.e. $\alpha_\infty \neq 0$, which indicated that racemization was not responsible for the observed changes. In addition, the corresponding visible absorption maximum did not change significantly over this time interval. A possible explanation for these observations is given in Scheme 1. The fact that the absorption maximum was unaffected indicates that hexadentately coordinated complexes were dominant in solution. Penta- and tetraamine copper(II) complexes invariably exhibit visible electronic maxima at significantly higher energy ($\bar{\nu}_{max} \sim 18\,000$–$20\,000$ cm^{-1}) relative to CuN_6 analogues, so their presence in these systems would have been apparent in the solution visible spectrum. Moreover, the pH independence of the process rules out a mechanism involving protonation of one or more coordinated amines, to afford penta- or tetradentate coordinated species.

The overall CD activity of the molecule arises from contributions from the chirotopic Cu center and six N-donors in addition to the conformation (*lel* or *ob*) of the three five-membered chelate rings. As there was no evidence for any species other than a CuN_6 complex, we contend that a relatively slow equilibrium is being established between conformational isomers of $[Cu\{(NMe_3)_2sar\}]^{4+}$ on the basis of the conformation of their five-membered chelate rings. A precedent for change in the CD spectrum as a function of the chirality of the five-membered chelate rings was established in the related Co(III) chemistry

(31) Day, P., Ed. *Electronic States of Inorganic Compounds: New Experimental Techniques*; D. Reidel Publishing Co.: Dordrecht, Boston, 1975.
(32) Isaacs, N. W.; Kennard, C. H. L. *J. Chem. Soc. A*, **1969**, 386.
(33) Joesten, M. D.; Hussain, M. S.; Lenhert, P. G. *Inorg. Chem.* **1970**, *9*, 151.
(34) Hathaway, B. J.; Dudley, R. J.; Nicholls, P. *J. Chem. Soc. A*, **1969**, 1845.
(35) Koch, R. C.; Joesten, M. D. *J. Chem. Phys.* **1973**, *59*, 6312.
(36) Bertini, I.; Gatteschi, D.; Scozzafava, A. *Inorg. Chem.* **1977**, *16*, 1973.
(37) Palmer, R. A.; Chin-Lan Yang, M. *Chem. Phys. Lett.* **1975**, *31*, 492.

Table 4. Predicted (MM) and Observed Cu−N Bond Lengths (Å) for (Hexaamine)copper(II) Complexes

	d_o, Å	d_{eq}, Å	d_{ax}, Å	TF
$[Cu(tach)_2](ClO_4)_2$[a]	2.17	**2.070(9)**	**2.353(7)**	**0.88**
$[Cu(tach)_2](NO_3)_4$[a]	2.17	2.164(3)	2.173(6)	1.0
MM	2.17	2.076	2.347	0.88
$[Cu(taci)_2]Br_2$[b]	2.17	2.086(4)	2.322(6)	0.90
MM	2.16	2.074	2.343	0.89
$[Cu(en)_3]Cl_2$[c]	2.16	**2.04(8), 2.11(8)**	**2.34(8)**	**0.89**
$[Cu(en)_3]SO_4$, 298 K[d]	2.15	2.150(2)	2.150(2)	1.0
$[Cu(en)_3]SO_4$, 120 K[c]	2.16	2.22(2)	2.055(2)	1.08
$[Cu(en)_3]^{2+}$, soln[e]	2.14	2.04(1)	2.34(2)	0.87
MM	2.17	2.065, 2.067	2.361	0.88
$[Cu(tacn)_2](ClO_4)_2$[f]	2.17	2.13(4)	2.233(7)	0.95
$[Cu(tacn)_2][Cu(CN_3]$, 293 K[g]	2.15	2.111(9)	2.228(6)	0.95
$[Cu(tacn)_2][Cu(CN_3]$, 110 K[g]	2.15	**2.06(1)**	**2.32(2)**	**0.89**
MM	2.16	2.070	2.323	0.89
$[Cu\{(NH_3)_2sar\}](NO_3)_4$[h]	2.17	2.088(3)−2.148(3)	2.251(3), 2.298(4)	0.93
MM	2.17	2.063, 2.089	2.348	0.88
$[Cu\{(NMe_3)_2sar\}](ClO_4)_4$[h]	2.17	2.17(1)	2.17(1)	1.0
MM	2.16	2.055, 2.083	2.337	0.89
$[Cu(pn)_3]br_2$[i]	2.16	2.09	2.31	0.90
MM	2.17	2.069(5)	2.358(1)	0.88
$[Cu(Me_5\text{-}N_6\text{-tricosane})](ClO_4)_2$[j]	2.18	2.22(2)	2.09(2)	1.06
MM	2.17	2.087(6)	2.339(9)	0.89

[a] Reference 6. [b] Hegetschweiler, K.; Gramlich, V.; Ghisletta, M.; Samaras, H. *Inorg. Chem.* **1992**, *31*, 2341. [c] Bertini, I.; Dapporto, P.; Gatteschi, D.; Scozzafava, A. *J. Chem. Soc., Dalton Trans.* **1979**, 1409. [d] Reference 30. [e] Inada, Y.; Ozutsumi, K.; Funahashi, S.; Soyama, S.; Kawashima, T.; Tanaka, M. *Inorg. Chem.* **1993**, *32*, 3010. [f] Beveridge, A. D.; Lavery, A. J.; Walkinshaw, M. D.; Schröder, M. *J. Chem. Soc., Dalton Trans.* **1987**, 373. [g] Reference 7. [h] This work. [i] Okamoto, T.; Matsumoto, K.; Kuroya, H. *Bull. Chem. Soc. Jpn.* **1970**, *43*, 1915. [j] Ralph, S. F.; Sargeson, A. M.; White, A. H. Unpublished results. [k] Values in bold type refer to structures used in the parametrization. Ligand structures are as follows:

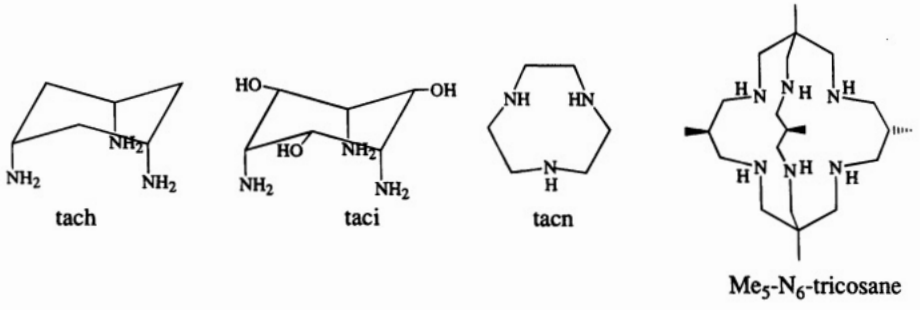

Scheme 1

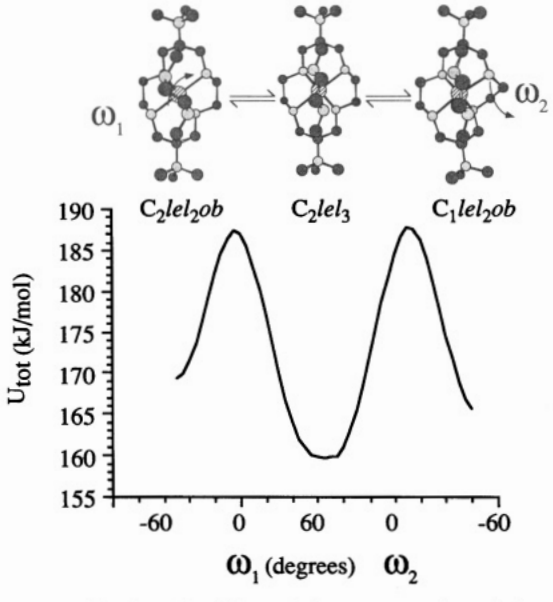

where a predominantly *lel* to *ob* interconversion of the five-membered chelate rings of $[Co\{(NH_3)_2sar\}]^{5+}$ was achieved by permethylation of the apical amines. The resulting CD of $[Co\{(NMe_3)_2sar\}]^{5+}$ (in a mainly *ob* condition) was essentially inverted relative to the spectrum of the precursor for the same absolute configuration about the metal center and six N-donors.[10] Strain energy minimization studies allow the classical barrier height for the interconversion of *lel* and *ob* conformers to be estimated.[38] In this case, a barrier of *ca.* 30 kJ mol^{-1} was determined, and the plot of strain energy of the complex as a function of the NCCN dihedral angle of the relevant chelate ring is also shown in Scheme 1. Although this barrier is somewhat higher than those found typically in analogous Co(III) complexes,[38] the observed rate for the change in optical rotation is still several orders of magnitude slower than one would anticipate. It is likely that the overall mechanism is more complicated than that proposed, but further speculation seems unwarranted without further investigation of the mutarotation.

Structural Aspects. The degree to which the crystallographically observed geometry of a given CuN_6 core is averaged may be gauged by the tetragonality factor TF = d_{eq}/d_{ax}, where d_{eq} and d_{ax} are the respective four short (or long) and two long (or short) Cu−L bonds in the tetragonally elongated (or compressed) complex. For TF < 1, the CuN_6 core will be tetragonally elongated, for TF > 1, the structures will appear tetragonally compressed, and for TF ≈ 1 the six Cu−N bonds will be approximately equal. Inspection of Table 4 reveals that TF reaches a minimum around 0.87 for structures where the genuine tetragonally elongated geometry of the complex was

(38) Hambley, T. W. *J. Comput. Chem.* **1987**, *8*, 651.

revealed. The intermediate value of TF = 0.93 for $[Cu\{(NH_3)_2sar\}](NO_3)_4$ indicates that this structure, although tetragonally distorted, is partially averaged, a result consistent with the temperature variability of the EPR spectrum.

It is anticipated that a low-temperature X-ray crystal structure analysis of $[Cu\{(NH_3)_2sar\}](NO_3)_4 \cdot H_2O$ may reveal an even more tetragonally distorted geometry. Variations in tetragonality as a function of temperature have been found in the structures of other (hexaamine)copper(II) complexes where the complex cation is located on a general site, the most notable example being $[Cu(tacn)_2][Cu(CN)_3]$.[7] Both $[Cu\{(NH_3)_2sar\}](NO_3)_4 \cdot H_2O$ and $[Cu(tacn)_2][Cu(CN)_3]$ represent examples of behavior of the type shown in Figure 2c, where dominant population of the lowest energy minimum is only achieved at low temperatures. By contrast, the crystallographic 3-fold symmetry of $[Cu\{(NMe_3)_2sar\}](ClO_4)_4$ dictates that an equal number of the three equivalent static distorted geometries are present at all temperatures (Figure 2a).

In an effort to probe the structural aspects concerning the underlying distorted geometries of (hexaamine)copper(II) complexes, we have modeled the complexes in Table 4 with molecular mechanics. The presence of Jahn–Teller coupling in the electronic ground state requires a different approach to modeling complexes such as these. That is, one cannot adopt the usual treatment that all bonds to chemically and symmetrically equivalent ligands are equal. We have previously modeled tetragonal $CuN_2O_2O'_2$ species by treating the axial Cu–O′ bonds differently from those in the equatorial CuN_2O_2 plane.[17] In this work, we have adopted a similar approach, whereby the strain-free Cu–N bond lengths for the equatorial and axial positions are different. Only crystal structures revealing the genuine tetragonally distorted geometry (TF < 0.9) were used in deriving the force field parameters, and these structures are given in bold type in Table 4.

Once these structures had been modeled satisfactorily, the remaining structures which exhibited averaged geometries were modeled. Inspection of the strain-energy-minimized structures indicates that the geometries of their CuN_6 cores are all rather similar, except those for $[Cu\{(NH_3)_2sar\}]^{4+}$ and $[Cu\{(NMe_3)_2sar\}]^{4+}$ which display a large trigonal twist distortion (~29°) superimposed on the anticipated tetragonal elongation. Note that averaging of the observed structures of $[Cu\{(NH_3)_2sar\}]^{4+}$ and $[Cu\{(NMe_3)_2sar\}]^{4+}$ did not affect the trigonal twist angle, which was essentially the same in the predicted tetragonally elongated geometries. This large trigonal twist results in a reduction in the energies of their visible maxima relative to those of the remaining complexes in Table 3, as expected from angular overlap model (AOM) studies of other hexaamine complexes.[39]

Static and Dynamic Jahn–Teller Effects. The EPR spectral behavior of $[Cu(Zn)\{(NMe_3)_2sar\}](ClO_4)_4$ was consistent with an equal population of the three symmetry-related, tetragonally elongated static distortions lying at the minima of the warped "Mexican hat" potential energy surface (Figure 2a). Between 20 and 170 K, it appears that the geometries are essentially static, as the positions of the resonances observed at 20 K are unaltered at the higher temperature. This allows one to estimate a lower limit for the barrier height (Figure 2a) of $B > 100$ cm^{-1}. Above 170 K, the spectrum narrows and partial dynamic behavior becomes apparent. As the dynamic process becomes dominant, the g and A values should approach their isotropic values, i.e. $g_{iso} \approx 2.12$ and $A_{iso} \approx 70$ G, but the latter is not resolved in the higher temperature spectra as the increase in spin–lattice relaxation rates at high temperature leads to the loss of resolution of hyperfine coupling. It has been shown[40] that line shape analysis of the EPR spectrum as a function of temperature may give an indication of the barrier height between the minima (Figure 2a). In this case, the relatively poor resolution of the spectra did not permit a similar analysis of the line widths.

The temperature variability of the g and A values in the EPR spectrum of $[Cu(Zn)\{(NH_3)_2sar\}](NO_3)_4 \cdot H_2O$ is consistent with behavior of type c in Figure 2. As illustrated in the crystallographic studies of $[M\{(NH_3)_2sar\}](NO_3)_4 \cdot H_2O$ (Cu, Zn), crystal packing forces lower the C_{3v} symmetry of the potential energy surface, stabilizing one minimum relative to the remaining two. An estimation of the energy difference between the lower energy and the higher energy minima in Figure 2c (ΔE) may be made from a Boltzmann distribution analysis based on variations in the $g_{\|}$ or $A_{\|}$ values as a function of temperature, providing that one knows the static, low-temperature values. In the case of $[Cu(Zn)\{(NH_3)_2sar\}](NO_3)_4$, the minimum of the temperature variation in $g_{\|}$ and $A_{\|}$ had not been reached at 20 K, (i.e., the complex was still exhibiting dynamic behavior at this temperature), so EPR spectroscopy could not be used to determine ΔE in this case.

The temperature variability of the EPR spectrum of $[Cu(Zn)\{(NH_3)_2sar\}](NO_3)_4$ points to the 295 K crystal structure determination as being representative of a partially averaged (dynamic) CuN_6 core. Variations in the observed Cu–N bond lengths as a function of temperature may also be used to gauge the relative populations of the three wells in Figure 2c.[7] The observed axial and equatorial Cu–N bond lengths, $\langle d_{ax} \rangle$ and $\langle d_{eq} \rangle$, their equivalent static bond lengths, d_{ax} and d_{eq}, and the relative populations of the lower energy (a) and two degenerate higher energy wells (b) (where $a + 2b = 1$) are related by eq 2. Following this approach and employing the Cu–N bond

$$b = 0.5(d_{ax} - \langle d_{ax} \rangle)/(d_{ax} - d_{eq}) = (\langle d_{eq} \rangle - d_{eq})/(d_{ax} - d_{eq}) \quad (2)$$

lengths obtained from the molecular mechanics calculation, which should represent the static distorted structure, one arrives at a relative population of 75% of the lower energy well at 293 K.

Visible–Near-IR Spectroscopy. A number of features of the electronic spectra are consistent with a strong tetragonal elongation in the Cu(II) chromophores. As previously indicated, in octahedral symmetry, Cu(II) d^9 has a ^2E_g ground state and a $^2T_{2g}$ excited state, separated by 10 Dq. We interpret the near-IR transition as the $^2A \leftarrow {}^2B$ transition state (^2E_g parentage) of a tetragonally elongated and trigonally twisted chromophore in C_2 symmetry, arising from the $d_{z^2} \leftarrow d_{x^2-y^2}$ orbital jump. Note that the tetragonal component of the ligand field potential is responsible for the splitting of the e_g orbitals, whereas the trigonal component is not (Figure 7). We then consider the visible band to comprise transitions to three components of a parent $^2T_{2g}$ state split by the combined effects of tetragonal and trigonal fields and spin–orbit coupling. Two components separated by ca. 700–1000 cm^{-1} were identified by CD and polarized absorption experiments and confirmed by MCD spectroscopy. It appears that two of the three components of this envelope exhibit CD transitions of similar energy, sign, and intensity, so separation of the visible envelope into its three anticipated components was not possible from the available data.

AOM calculations based on the strain-energy-minimized geometry of the $[Cu\{(NR_3)_2sar\}]^{4+}$ (R = H, CH_3) chromophore point to the trigonal splitting of the $^2T_{2g}$ (O_h) state (yielding ^2E and $^2A_1$ (D_3) states) being ~1500 cm^{-1} as a result of the trigonal

(39) Bernhardt, P. V.; Comba, P. *Inorg. Chem.* **1993**, *32*, 2798.

(40) Hudson, A. *Mol. Phys.* **1966**, *10*, 575.

twist distortion (φ = 28°) (Figure 7). In the absence of tetragonal distortion, i.e. purely trigonal symmetry, two closely spaced visible transitions ($^2A_1 \leftarrow {}^2E$ and $^2E \leftarrow {}^2E$) should have been observed in the vis-near-IR spectrum. Therefore, the lower energy $^2A \leftarrow {}^2B$ transition is a direct indicator of the magnitude of the tetragonal field in this chromophore. This transition has strongly variable electric dipole intensity in tetragonally compressed, elongated, and cubic environments.[41,42] It becomes more intense as the axial and equatorial ligands become inequivalent and almost vanishes in a cubic environment. Furthermore, this transition does not have magnetic dipole transition intensity in first order. This is consistent with the observation of weak CD of the near-IR band in Figure 9.

A difficulty lies in the understanding of the intensity mechanisms for the transitions in this system. The polarization behavior seen in Figure 8 is not compatible with electric dipole selection rules for the anticipated tetragonally elongated, C_2 symmetric chromophore, where the principal axis of the molecule would be perpendicular to the crystal c axis. The near-IR ($^2A \leftarrow {}^2B$) transition should be electric dipole allowed both perpendicular and parallel to the principal (C_2) axis of the tetragonally elongated molecule, which is parallel and perpendicular to the crystal c axis, respectively. However, this transition is quite strongly σ polarized (>5:1). The three components of the visible maximum comprise two $^2A \leftarrow {}^2B$ transitions and one $^2B \leftarrow {}^2B$ transition, the latter of which should be σ polarized, continuing with the trigonal definition of the polarization directions. Regardless of the origin of these observations, the data are unequivocal in defining the near-IR transition as being strongly polarized perpendicular to the "trigonal" direction of the ligand, whereas the visible transitions have significant intensity both parallel and perpendicular to this trigonal direction.

Given that the solution spectroscopic behaviors of $[Cu\{(NMe_3)_2sar\}]^{4+}$ and $[Cu\{(NH_3)_2sar\}]^{4+}$ are essentially the same, it is reasonable to assume that the known polarization properties of $[Cu\{(NMe_3)_2sar\}]^{4+}$ are the same for $[Cu\{(NH_3)_2sar\}]^{4+}$ at the molecular level. Recall that the orientation of the $[Cu\{(NH_3)_2sar\}](NO_3)_4 \cdot H_2O$ crystal with respect to the incident radiation was uncertain, so the polarization directions could not be determined explicitly. Examination of the (100), (010), and (001) projections of the unit cell of $[Cu\{(NH_3)_2sar\}](NO_3)_4 \cdot H_2O$ reveals that the "trigonal" axes of the ligands are parallel with the (010) face and oriented such that they are approximately 30° to the (100) face. If the incident radiation in the 300 K polarized spectra was perpendicular to the (001) face and the perpendicular and parallel electric vector directions were relative to the a axis, one would expect the ratio of $A(E \perp)/A(E \parallel) = 4/3$ ($\approx$1.3), assuming that the near-IR transition has negligible intensity parallel to the "trigonal" axis of the ligand. The experimental ratio is 1.6. It can be shown by similar arguments that the absorbance ratios $A(E \perp)/A(E \parallel)$ would be 3 and 4 for the incident radiation perpendicular to the (010) and (100) planes respectively. (Details of these calculations have been deposited as supplementary material.) On this basis, it emerges that the crystal was oriented with its (001) face normal to the incident light. Moreover, the electric vector directions were relative to the a axis, otherwise the intensity ratio would have been inverted; i.e., $A(E \perp)$ would have been less than $A(E \parallel)$.

The intensity of the near-IR transition in the single-crystal polarized absorption spectrum of $[Cu\{(NH_3)_2sar\}](NO_3)_4$ (Figure 10) increases significantly with cooling, yet the MCD is quite unambiguous in requiring significant vibronically induced intensity of the related $[Cu\{(NMe_3)_2sar\}](ClO_4)_4$ chromophore (Figure 11). A vibronic process normally leads to a decrease of intensity with cooling. We speculate that although the many features of the system such as band positions and g values are determined largely by the tetragonal component of the field associated with the Jahn–Teller process, the intensities are more subtly related to the trigonal potential in the complex. A more careful analysis of the MCD spectra in Figure 11 may provide some estimate of the effect of a trigonal potential in this system.

Conclusions

Although the majority of transition metal complexes of (NH_2)-sar exhibit trigonally distorted octahedral MN_6 geometries, it was found that $[Cu\{(NH_3)_2sar\}]^{4+}$ and $[Cu\{(NMe_3)_2sar\}]^{4+}$ display, additionally, tetragonally distorted structures both in solution and in the solid state, as a result of strong Jahn–Teller coupling. The trigonal crystallographic site symmetry of $[Cu\{(NMe_3)_2sar\}](ClO_4)_4$ was connected with disorder of the tetragonally distorted molecule around the pseudo 3-fold axis. A tetragonally elongated geometry of the cation in $[Cu\{(NH_3)_2sar\}](NO_3)_4$ was revealed in its crystal structure, but its strongly temperature-dependent EPR behavior was indicative of its 295 K structure being partially averaged. Molecular mechanics calculations indicated that the underlying static geometry was indeed more tetragonally distorted than that seen in the 295 K structure of $[Cu\{(NH_3)_2sar\}](NO_3)_4$. Single-crystal polarized vis-near-IR spectroscopy revealed that intensity mechanisms in the electronic transitions of these systems appear to be connected with the trigonal directions of the macrobicyclic ligands and not along the tetragonal directions of the CuN_6 core. Although the d–d transitions are quite intense, they have considerable vibronically induced character as shown from their temperature dependence in the absorption and MCD spectra.

In the absence of these special electronic properties, the isomorphous Zn(II) analogues of both complexes display the expected trigonal symmetry in solution and in the solid state. The presence of the pendent primary ammonio or trimethylammonio groups has little effect on the spectral properties of the complexes relative to their $[M(sar)]^{2+}$ parents, but dramatic stabilization of the tetrapositively charged complexes toward acid-catalyzed dissociation and racemization results.

Acknowledgment. The Australian Research Council is gratefully acknowledged for financial support. We also thank Dr. M. J. Riley and Dr. L. Dubicki for helpful discussions and D. Bogsanyi for technical assistance.

Supplementary Material Available: Tables of atomic coordinates, thermal parameters, ligand and anion bond lengths and bond angles, and H atom positional and thermal parameters and polarization projection diagrams (24 pages). Ordering information is given on any current masthead page.

IC941372+

(41) Riley, M. J.; Dubicki, L.; Moran, G. M.; Krausz, E. R.; Yamada, I. *Inorg. Chem.* **1990**, *29*, 1614.
(42) Dubicki, L.; Riley, M. J.; Krausz, E. R. *J. Chem. Phys.* **1994**, *101*, 1930.